J Mater Sci (2009) 44:6663–6669
DOI 10.1007/s10853-009-3582-9

MESOSTRUCTURED MATERIALS

Mesoporous $Ce_{0.8}Zr_{0.2}O_2$ solid solutions-supported CuO nanocatalysts for CO oxidation: a comparative study of preparation methods

Jian-Liang Cao · Qing-Fang Deng · Zhong-Yong Yuan

Received: 29 November 2008 / Accepted: 12 May 2009 / Published online: 28 May 2009

Abstract $Ce_{0.8}Zr_{0.2}O_2$ solid solutions were prepared by three different methods, namely, surfactant-assisted, co-precipitation, and sol–gel methods, and were used as supports of CuO nanocatalysts by the deposition-precipitation (DP) method. The prepared supports and catalysts were characterized by using XRD, N_2 adsorption, TEM, and H_2-TPR techniques. The influence of preparation methods on the low-temperature carbon monoxide oxidation activity of these $CuO/Ce_{0.8}Zr_{0.2}O_2$ catalysts was investigated comparatively by using a microreactor-GC system. The catalyst prepared by surfactant-assisted method is more active for low-temperature CO oxidation than the ones prepared by the co-precipitation and sol–gel methods. The support and catalysts prepared by surfactant-assisted method possess mesoporous framework, nanoscale particle size, and high surface area, improving the synergistic effect between CuO species and support, which is beneficial for enhancing the catalytic performance of low-temperature CO oxidation.

Introduction

As one of the most active transition metal oxide catalysts for emission control reactions [1–10], copper oxide-based catalysts are useful for the total oxidation of CO [5–8, 10, 11], hydrocarbon [4, 12, 13], chlorinated hydrocarbons, and alcohols [14, 15]. Thus, supported copper oxide catalysts have attracted much attention as an alternative to either reduce the usage of or even replace these noble metal-based emission control catalysts [16]. The suitable supports for these supported catalysts on low-temperature CO oxidation are the metal oxides that could be partially reduced, such as CeO_2, Fe_2O_3, and TiO_2 [6, 7, 17].Out of these metal oxides, cerium dioxide is of great interest because of its oxygen storage and release properties. However, the pure CeO_2 has poor thermal stability. Doping the CeO_2 lattice with ZrO_2 can lead to improvement in oxygen storage capacity, redox property, and thermal resistance and will form a Ce–Zr–O solid solution [18–21], resulting in better performance in CO oxidation [22] and combustion of methane [23]. Out of all the Ce–Zr–O solid solutions with different Ce/Zr ratio, $Ce_{0.8}Zr_{0.2}O_2$ was the most texturally stable one [24].

Since the preparation method can strongly affect the catalytic activity of the Ce–Zr–O solid solution on low-temperature CO oxidation, water–gas shift reaction, and preferential oxidation of CO in excess hydrogen, many methods have been reported for the preparation of Ce–Zr–O solid solution, such as microwave method [25], co-precipitation [11, 26–28], sol–gel technique [22, 29], surfactant-assisted method [5]. Dong et al. [30] investigated the activities of $CuO–CeO_2–ZrO_2$ catalysts synthesized by four methods, namely, sol–gel, co-precipitation, one-step impregnation, and two-step impregnation, for CO removal from hydrogen-rich gas. They found that the co-precipitation-prepared sample exhibited the best catalytic performance. Our previous reports [5] show that the surfactant-assisted one-step-prepared $CuO/Ce_{0.8}Zr_{0.2}O_2$ catalysts possess mesoporous structure and exhibited high catalytic activity for low-temperature CO oxidation. Obviously, the preparation methods had a marked effect on the behavior of

J.-L. Cao · Q.-F. Deng · Z.-Y. Yuan (✉)
Institute of New Catalytic Materials Science, Key Laboratory of Energy-Material Chemistry (Tianjin) & Engineering Research Center of Energy Storage and Conversion (Ministry of Education), College of Chemistry, Nankai Unviersity, Tianjin 300071, People's Republic of China
e-mail: zyyuan@nankai.edu.cn

$CuO–CeO_2–ZrO_2$ catalysts in catalytic oxidation of CO, and developing high-surface-area and mesoporous $Ce_{0.8}Zr_{0.2}O_2$ solid solution and $CuO/Ce_{0.8}Zr_{0.2}O_2$ catalysts for the anticipation of enhancing catalytic performance requires significant work.

In the present work, $Ce_{0.8}Zr_{0.2}O_2$ solid solutions were prepared by three different methods, namely, surfactant-assisted, co-precipitation, and sol–gel methods, and their CuO-loaded nanocatalysts were prepared by the deposition-precipitation (DP) method. The textural and structural properties of the prepared $Ce_{0.8}Zr_{0.2}O_2$ supports and $CuO/Ce_{0.8}Zr_{0.2}O_2$ nanocatalysts were characterized by means of XRD, N_2 sorption, TEM, and H_2-TPR techniques. The influence of the prepared methods on the low-temperature CO oxidation activities were investigated in detail.

Experimental

Catalyst preparation

The $Ce_{0.8}Zr_{0.2}O_2$ solid solutions were prepared by three different methods, namely, surfactant-assisted method (denoted as SA), sol–gel method (denoted as SG), and co-precipitation method (denoted as CP). All the supported CuO nanocatalysts were prepared by the deposition-precipitation method, and the catalysts were denoted as CuO/SA, CuO/SG, and CuO/CP, respectively.

The SA $Ce_{0.8}Zr_{0.2}O_2$ solid solution was synthesized as follows: at room temperature, 6 mmol of cetyltrimethylammonium bromide (CTAB) was dissolved into 200 mL distilled water under ultrasound irradiation for 15 min, then 8 mmol of $Ce(NO_3)_3 \cdot 6H_2O$ and 2 mmol of $Zr(NO_3)_4 \cdot 5H_2O$ were added under vigorous stirring. After stirring for 0.5 h, 0.2 mol/L sodium hydroxide solution was gradually added into the above solution until the pH value of the mixed solution was 10, and then further stirred for about 12 h. The final suspended solution was aged at 90 °C for 3 h, washed with hot water, dried in the oven at 110 °C for 6 h, and then milled and calcined at 400 °C for 4 h.

The SG $Ce_{0.8}Zr_{0.2}O_2$ solid solution was synthesized starting from nitrate precursors and citric acid. At room temperature, 24 mmol $Ce(NO_3)_3 \cdot 6H_2O$ and 6 mmol $Zr(NO_3)_4 \cdot 5H_2O$ were dissolved into 300 mL distilled water, and 15 mmol citric acid was slowly added into the above solution under vigorous stirring. After stirring for 1 h, the solution was heated at 90 °C to vaporize the water until it was about dried, dried in the oven at 110 °C for 6 h, and then milled and calcined at 400 °C for 4 h.

The CP $Ce_{0.8}Zr_{0.2}O_2$ solid solution was prepared by using $Ce(NO_3)_3 \cdot 6H_2O$, $ZrOCl_2 \cdot 8H_2O$ and NH_4OH. At room temperature, 30 mmol $Ce(NO_3)_3 \cdot 6H_2O$ and 7.5 mmol $ZrOCl_2 \cdot 8H_2O$ were dissolved into 200 mL distilled water under vigorous stirring, and 2 mol/L NH_4OH aqueous solution was added dropwise until the pH of the solution was 9. The solution was further stirred for 2 h and then centrifuged and washed several times with deionized water and ethanol until Cl^- could not be examined by 0.1 mol/L $AgNO_3$ aqueous solution. The obtained precipitate was dried at 110 °C for 6 h, and then milled and calcined at 400 °C for 4 h.

The supported CuO nanocatalysts, CuO/SA, CuO/SG, and CuO/CP, were prepared by the deposition-precipitation (DP) method. At room temperature, 1 g $Ce_{0.8}Zr_{0.2}O_2$ support was first suspended in the aqueous solution of an appropriate amount of $Cu(NO_3)_2 \cdot 3H_2O$. Then, 0.25 mol/L of Na_2CO_3 solution was gradually added into the above suspended solution until the pH value of the mixed solution reached 9.0. After stirring for 1 h, the mixture was filtered and washed with distilled water. The obtained solid was dried at 80 °C for 4 h and subsequently calcined at 400 °C for 3 h. The loading amount of CuO was denoted as *x*%.

Catalyst characterization

X-ray diffraction (XRD) analysis was performed on a Rigaku D/max-2500 diffractometer, with CuKα radiation at 40 kV and 100 mA in a scanning range of 3 to 80° (2θ). The diffraction peaks of the crystalline phase were compared with those of standard compounds reported in the JCPDS Date File. The average crystallite size was calculated from the peak width using the Scherrer's equation.

N_2 adsorption-desorption isotherms were collected at liquid nitrogen temperature using a Quantachrome NOVA 2000e sorption analyzer. The specific surface areas (S_{BET}) of the samples were calculated following the multi-point BET (Brunauer–Emmett–Teller) procedure. The pore size distributions were determined by using both the BJH (Barett–Joyner–Halenda) method and the NLDFT (non-local density functional theory) modeling method. Before carrying out the measurement, each sample was degassed at 200 °C for more than 6 h.

Transmission electron microscopy (TEM) analysis was performed on a Philips Tecnai G20 microscope, operating at 200 kV. The samples were dispersed in ethanol and treated with ultrasound for 5 min, and then deposited on a copper grid coated with preformed holey carbon film.

Temperature-programmed reduction (TPR) experiments were performed under the mixture of 5% H_2 in N_2 flowing (30 mL/min) over 50 mg of catalyst at a heating rate of 10 °C/min. The uptake amount during the reduction was measured by using a thermal conductivity detector (TCD). For comparison, H_2-TPR measurement of pure CuO was carried out over 7.4 mg of CuO powder.

Catalytic activity testing

Catalytic activity tests were performed in a continuous-flow fixed-bed microreactor. A stainless steel tube with an inner diameter of 7 mm was chosen as the reactor tube. About 200 mg catalyst power was placed into the tube. The reaction gas mixture consisting of 10 vol.% CO balanced with air was passed through the catalyst bed at a total flow rate of 36.6 mL/min. A typical weigh hourly space velocity (WHSV) was 11,000 mL/h/g. After 30 min reaction, the effluent gases were analyzed online by a GC-900A gas chromatograph equipped with a thermal conductivity detector (TCD). The activity was expressed by the conversion of CO.

Results and discussion

Catalyst characterization

X-ray diffraction analysis

Figure 1 shows the X-ray diffraction patterns of the $Ce_{0.8}Zr_{0.2}O_2$-supported 12%-CuO catalysts prepared by different methods. The main reflections at 28.8, 33.3, 47.9, and 56.8° of 2θ in the XRD patterns of all the samples correspond to the cubic fluorite structure, typical of CeO_2. This indicates that the zirconia dopant is contained within the CeO_2 lattice to form a solid solution while maintaining the fluorite structure [5]. The mean particle sizes of $Ce_{0.8}Zr_{0.2}O_2$ support, calculated by the Scherrer's equation, are listed in Table 1. Of the three kinds of $Ce_{0.8}Zr_{0.2}O_2$, the particle size of the SG one is obviously the biggest. From Fig. 1, it can be seen that the diffraction peaks attributed to CuO crystal phase appeared at 35.5° and 38.7° for all these three catalysts and their intensity was very different. CuO, which was supported on the CP support, has the highest intensity. This means that in the CuO/CP catalyst the active species CuO has the biggest particle size, and this may result in lower catalytic activity in CO oxidation. Hence, we proposed that SA may be the suitable one as the catalyst support because of its small $Ce_{0.8}Zr_{0.2}O_2$ particle size which could render high surface area and high dispersion of copper species.

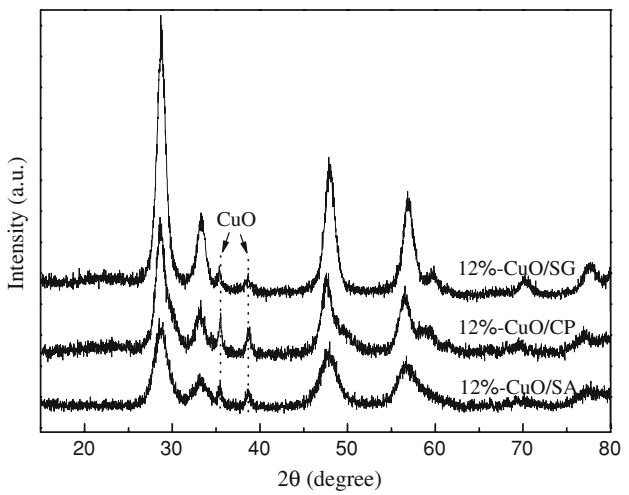

Fig. 1 XRD patterns of $Ce_{0.8}Zr_{0.2}O_2$-supported CuO nanocatalysts prepared by different methods

The XRD patterns of the *x*%-CuO/SA catalysts with different CuO loading amount are shown in Fig. 2. With the increase of the CuO loading amount, the diffraction peaks attributed to CuO crystal phase appeared at 35.5° and 38.7°. Moreover, when the CuO loading amount was below 8%, no characteristic reflections of CuO structure presented, which may be due to the high dispersion of the CuO nanoparticles with the particle sizes on the surface of the support being too small to be identified by the conventional X-ray diffraction method. When the CuO loading amount increased to 12%, the weak diffraction peaks attributed to CuO crystal phase appeared at 35.5° and 38.7°, suggesting the agglomeration of excess copper species and the growth of the CuO nanoparticles or the formation of bulk CuO. The average sizes of CuO particles, calculated from the CuO (111) reflection peak, are listed in Table 1.

N_2 adsorption analysis and transmission electron microscopy

The nitrogen adsorption-desorption isotherms and the corresponding pore size distributions of the $Ce_{0.8}Zr_{0.2}O_2$ support prepared by different methods and the *x*%-CuO/SA catalysts with different CuO loading amount are shown in Figs. 3 and 4; their textual properties are also listed in Table 1.

Figure 3 displays the nitrogen adsorption–desorption isotherms and the corresponding pore size distributions of the $Ce_{0.8}Zr_{0.2}O_2$ support prepared by different methods. The isotherms of both SA and CP samples are of classical type IV, characteristic of mesoporous materials according to the IUPAC classification. A hysteresis loop with a sloping adsorption branch and a relatively sharp steep desorption branch is observed at high relative pressure (P/P_0) range. Usually such a well-defined hysteresis loop of H2-type could indicate that the effective radii of the mesoporous bodies are heterogeneously distributed and the effective radii of the narrow entrances are of equal size [31]. Actually, such hysteresis loops observed for these samples could also be indicative of cavitation induced evaporation, and need not only be caused by classical pore blocking/percolation. For cavitation to occur, all pore entrances need to be below a certain critical width/diameter, but their actual

Table 1 Comparison of particle sizes, textural properties, and catalytic activities for CO oxidation of $Ce_{0.8}Zr_{0.2}O_2$ and $CuO/Ce_{0.8}Zr_{0.2}O_2$ nanocatalysts prepared by different methods

Catalysts	Mean particle size of $Ce_{0.8}Zr_{0.2}O_2$ (nm)	Mean particle size of CuO (nm)	Surface area[a] (m^2/g)	Pore volume[b] (cm^3/g)	$D_{BJH\text{-}ads}$[c] (nm)	Average pore diameter[d] (nm)	D_{DFT}[e] (nm)	CO conversion T_{100} (°C)
SA	4.6	–	201	0.177	2.6	3.5	3.7	–
CP	5.7	–	119	0.120	2.9	4.0	3.6	–
SG	7.3	–	59	–	–	–	–	–
4%-CuO/SA	4.8	–	177	0.173	2.4	3.9	4.1	100
8%-CuO/SA	5.9	–	163	0.163	2.5	4.0	4.1	95
12%-CuO/SA	5.0	5.2	173	0.173	2.6	4.0	3.6	80
16%-CuO/SA	4.7	8.5	163	0.167	2.6	4.1	3.7	85
12%-CuO/CP	6.1	6.4	109	0.126	2.8	4.6	3.5	115
12%-CuO/SG	7.7	4.9	64	–	–	–	–	95

[a] Multi-point BET surface area

[b] Total pore volume at $P/P_0 = 0.99$

[c] Pore diameter determined by the BJH mode method

[d] Aaverage pore diameter (4 V/A)

[e] Pore diameter determined by the NLDFT modeling method

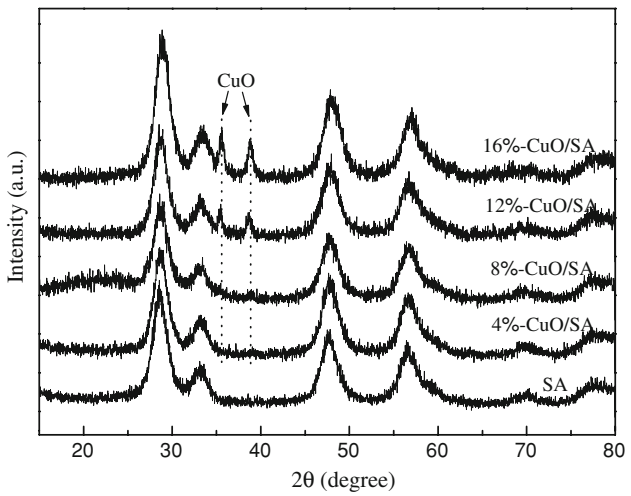

Fig. 2 XRD patterns of *x*%-CuO/SA nanocatalysts with different CuO loading amounts

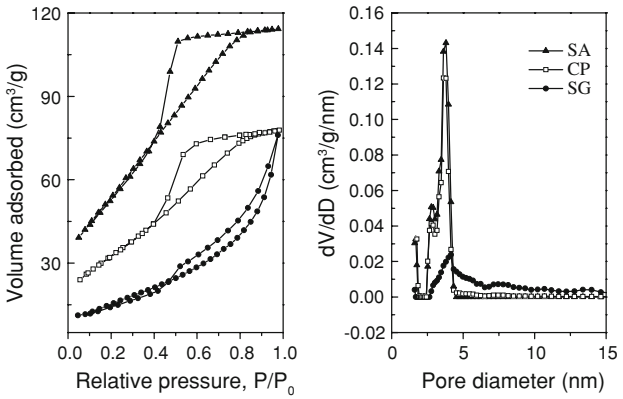

Fig. 3 (*left*) N_2 adsorption–desorption isotherms and (*right*) the corresponding NLDFT pore size distribution curves of $Ce_{0.8}Zr_{0.2}O_2$ solid solutions prepared by different methods

width/diameter can vary over a wide size range, i.e., the pore entrances need not be of equal (or similar) width to produce hysteresis loops with such steep desorption branches. The cavitation pressure (i.e., the pressure where desorption of capillary condensed liquid from the main pores occurs) depends on the thermophysical state of the capillary condensed liquid in the main pores but not on the size/width of the pore entrances. The H2-type of the hysteresis loop is typical for wormhole-like mesostructures and hierarchical scaffold-like mesoporous structures [31, 32]. The adsorption isotherms of the prepared samples exhibit a large increase in the P/P_0 range of 0.2 to 0.4, which is characteristic of capillary condensation within mesopores. As shown in Table 1, the specific surface area of SA is much higher than that of CP. The pore size distribution curves of the support SA and CP, determined by the BJH method from the adsorption branch of the isotherms, exhibit one single narrow peak centered at 2.3 nm and 2.4 nm, indicating the good homogeneity of the pores. Since the BJH method somewhat underestimated small mesopores, the NLDFT modeling method was also used to calculate the pore sizes of the materials, and the pore size distributions of 3.7 nm and 3.6 nm are obtained for the support SA and CP, respectively (Fig. 3). However, the sample SG did not possess uniform mesoporous structure. Figure 4 shows the

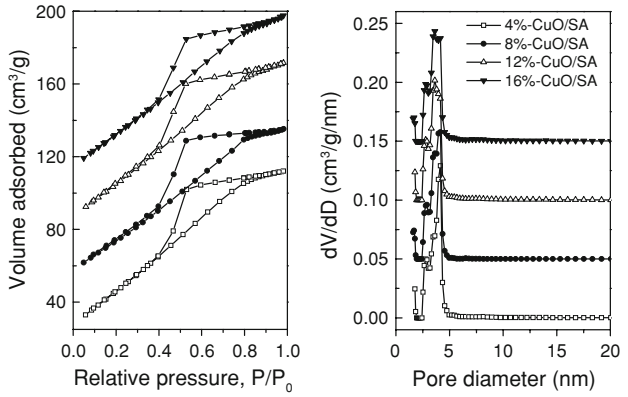

Fig. 4 (*left*) N_2 adsorption–desorption isotherms and (*right*) the corresponding NLDFT pore size distribution curves of the *x*%-CuO/SA nanocatalysts with different CuO loading amounts. The volume was shifted by 30, 60, and 90 and d*V*/d*D* value was shifted by 0.05, 0.10, and 0.15 for the curves of 8%- , 12%- , and 16%-CuO/SA, respectively

nitrogen adsorption–desorption isotherms and the corresponding NLDFT pore size distributions of the *x*%-CuO/SA catalysts with different CuO loading amount. The pore size distribution curves exhibit one single narrow peak from 3.7 nm to 4.1 nm with the increase of the CuO loading amount from 4% to 16%, which are comparable with that of pure SA support, indicating that the *x*%-CuO/SA catalysts maintained the porosity structure of the SA support after loading CuO. With the increase of the CuO loading amount from 4% to 16%, the surface area of the catalysts decreased from 201 m^2/g to 163 m^2/g (Table 1), accompanied by the decrease of the pore volume and pore size. This may be due to the agglomeration of the excessive CuO nanoparticles on the SA support.

Figure 5 shows the TEM micrograph of the 400 °C-calcined 12%-CuO/SA catalyst. The image clearly demonstrates that the catalyst has a disordered wormhole-like mesopore structure, formed by the agglomeration of the uniform nanoparticles. The accessible pores are connected randomly, lacking discernible long-range order in the pore arrangement among the small particles, which is consistent with the N_2 adsorption–desorption isotherms in Fig. 4. The nanoparticles in the catalyst are of regular spherical morphology with the size around 5 nm, consistent with the crystallite size obtained from XRD analysis.

H_2-TPR analysis

In order to determine the existence state of copper species and the interaction between CuO and $Ce_{0.8}Zr_{0.2}O_2$ support, the H_2-TPR analysis was performed. Figure 6 shows the typical H_2-TPR profiles of $Ce_{0.8}Zr_{0.2}O_2$-supported CuO catalysts prepared by different methods. Four reduction peaks (denoted as α, β, γ, and δ) are seen for mesoporous

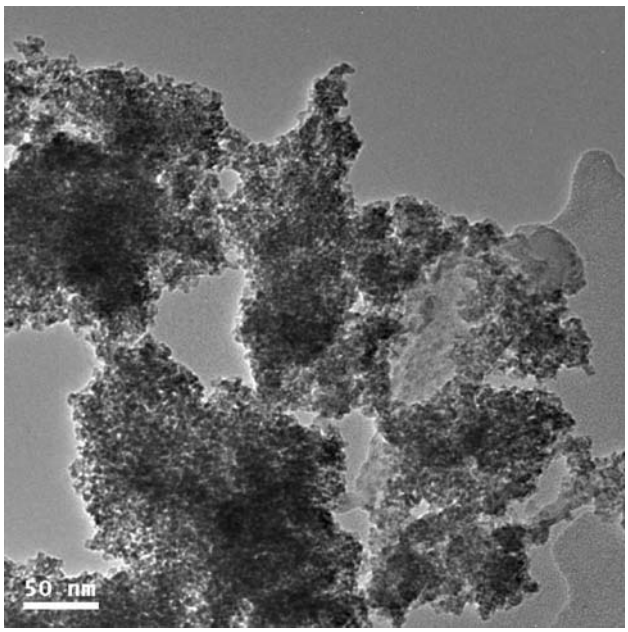

Fig. 5 TEM image of 12%-CuO/SA nanocatalyst

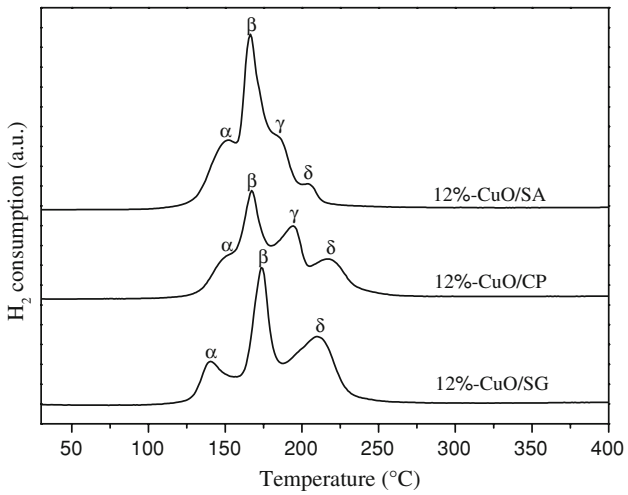

Fig. 6 H_2-TPR profiles of $Ce_{0.8}Zr_{0.2}O_2$-supported CuO nanocatalysts prepared by different methods

SA- and CP-supported CuO catalysts. However, there are only three peaks (denoted as α, β, and δ) for SG-supported CuO catalyst. It is known that pure CuO shows a single reduction peak of maximum hydrogen consumption at about 370 °C [5, 8, 33]. For all the CuO-loaded catalysts, the reduction peaks of CuO centered at the temperature lower than that of the pure CuO. This may be due to the synergistic effects between CuO and the $Ce_{0.8}Zr_{0.2}O_2$ support; $Ce_{0.8}Zr_{0.2}O_2$ can enhance the reducibility of the supported copper oxide. Zhou et al. [34] had studied the TPR and TPD behavior of CuO/ZrO_2 catalysts and found that there were five reduction peaks at 185, 220, 278, 360,

and 395 °C, of which three lower temperature peaks are ascribed to the reductions of highly dispersed copper species and two higher temperature peaks are ascribed to the reduction of bulk CuO. Avgouropoulos and Ioannides [35] reported that there were three overlapping reduction peaks presented in the CuO–CeO_2 catalyst: a low-intensity, low-temperature peak at 168 °C represented the reduction of copper species that strongly interacted with CeO_2 and two peaks of higher intensity at 210 °C and 255 °C were attributed to the reduction of larger CuO particles less associated with ceria. Our previous study [5] showed that there were two reduction peaks (186 °C and 223 °C) for the one-step synthesized mesoporous CuO/$Ce_{0.8}Zr_{0.2}O_2$ catalyst: the lower temperature peak was ascribed to the reduction of finely dispersed CuO species strongly interacting with the support, and the higher temperature peak was assigned to the reduction of Cu^{2+} ions incorporated into the lattice of the $Ce_{0.8}Zr_{0.2}O_2$ support. In the case of this study, the assignment of these peaks are as follows:

Peak α: 150, 151, and 140 °C peaks for these three catalysts are ascribed to the reduction of finely dispersed copper species strongly interacting with the $Ce_{0.8}Zr_{0.2}O_2$ support.

Peaks β and peak γ: peak β at 166, 167, and 174 °C for these three catalysts and peak γ at 189 °C and 195 °C for CuO/SA and CuO/CP catalysts are assigned to the reduction of larger CuO particles less associated with $Ce_{0.8}Zr_{0.2}O_2$ support.

Peak δ: centered at 206, 218, and 211 °C peaks represent the reduction of bulk CuO.

We can also see clearly from Fig. 6 that the intensity of peaks α, β, and γ in the reduction curve of CuO/SA catalyst is much higher than that of CuO/CP and CuO/SG catalysts. This indicates that there are much more active copper species on the surface of the high-surface-area SA support for the CuO/SA catalyst than that of the CuO/CP and CuO/SG catalysts. The abundant active copper species may result in high catalytic activity in low-temperature CO oxidation.

Catalytic activity

The catalytic activities of the prepared CuO/$Ce_{0.8}Zr_{0.2}O_2$ catalysts as a function of reaction temperature are investigated and the results are presented in Figs. 7 and 8. The results show a similar behavior; the CO oxidation activity of all the CuO/$Ce_{0.8}Zr_{0.2}O_2$ samples increased with the increase of the catalytic reaction temperature measured in the catalyst bed. The "light-off" temperature for 100% CO conversion of the catalysts is shown in Table 1.

Figure 7 shows the catalytic activity for CO oxidation of $Ce_{0.8}Zr_{0.2}O_2$-supported CuO catalysts, 12%-CuO/$Ce_{0.8}Zr_{0.2}O_2$ catalysts, prepared by different methods. It can be

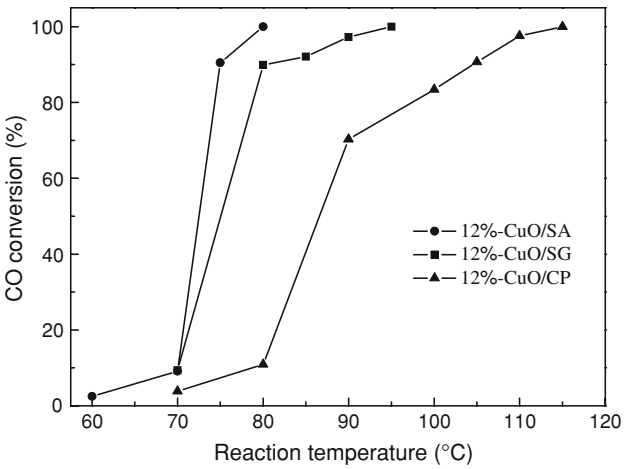

Fig. 7 Catalytic activity for CO oxidation of $Ce_{0.8}Zr_{0.2}O_2$-supported CuO catalysts prepared by different methods

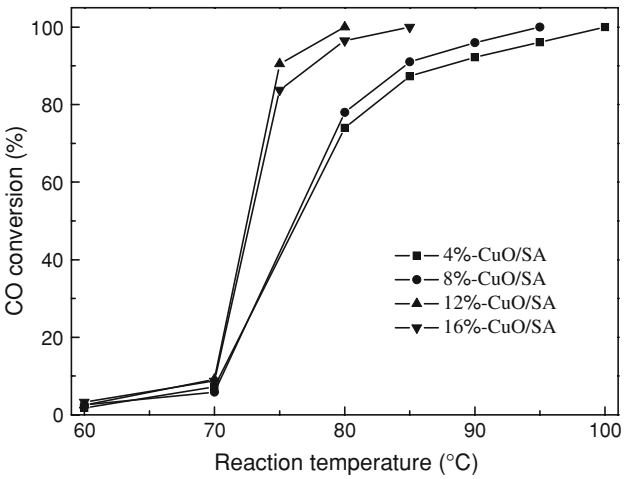

Fig. 8 Catalytic activity for CO oxidation of *x*%-CuO/SA nanocatalysts with different CuO loading amounts

seen that 12%-CuO/SA has the highest activity for CO total oxidation at 80 °C, which is much higher than the previously reported results [5, 11, 29]. However, the total CO conversion temperature T_{100} of 12%-CuO/SG and 12%-CuO/CP was 95 °C and 115 °C, respectively. The catalytic results were consistent with the XRD and N_2 adsorption data, indicating that the mesoporous framework, the high surface area, and the uniform distribution of nanoscale particle size of support were responsible for the high catalytic activity. The catalytic activity of *x*%-CuO/SA catalysts for CO oxidation is shown in Fig. 8. It is seen that the catalytic activity of *x*%-CuO/SA catalysts enhanced with the increase of CuO loading amount from 4% to 12%, and the 12%-CuO/SA catalyst exhibited the highest catalytic activity. However, further increase of the CuO loadings resulted in the decrease of the catalytic activity. This indicates that the finely dispersed CuO species should be responsible for the activity,

supported by the H_2-TPR and XRD results. With the high loading of CuO, the excess CuO species would not only cover some of the active sites, but also lead to the growth of CuO particles or bulk CuO formation, which may have a negative effect on the catalytic activity of low-temperature CO oxidation. On the other hand, the CuO particle size in 16%-CuO/SA is much larger than that in 12%-CuO/SA due to the excess of CuO, which may deteriorate the catalytic activity of the catalyst [5, 29]. Thus, the fine dispersion of CuO species on the high surface area support may have a positive effect on the catalytic activity of low-temperature CO oxidation and the 12% loading amount may be the feasible one.

Conclusions

In summary, $Ce_{0.8}Zr_{0.2}O_2$ prepared by three different methods (i.e., surfactant-assisted, co-precipitation, and sol–gel) and their CuO-loaded nanocatalysts have been comparatively examined with respect to their catalytic activity for low-temperature CO oxidation. The $CuO/Ce_{0.8}Zr_{0.2}O_2$ catalysts prepared by surfactant-assisted method possess mesoporous framework with narrow pore size distribution, uniform distribution of nanoscale particle size, and high specific surface area, and the 12%-CuO-loaded nanocatalyst has the highest catalytic activity for CO total oxidation at 80 °C. According to the catalytic activity measurements and the H_2-TPR analysis results we can also conclude that the synergistic effect between CuO and the $Ce_{0.8}Zr_{0.2}O_2$ solid solution support and the highly dispersed CuO nanoparticles are also responsible for the high catalytic activity of the catalysts in low-temperature CO oxidation. This surfactant-assisted method can also be used to synthesize other mesoporous metal oxide catalyst materials.

Acknowledgements This work was supported by the National Natural Science Foundation of China (No. 20473041 and 20673060), the National Basic Research Program of China (No. 2009CB623502), the Specialized Research Fund for the Doctoral Program of Higher Education (20070055014), the Natural Science Foundation of Tianjin (08JCZDJC21500), the Program for New Century Excellent Talents in University (NCET-06-0215), and Nankai University.

References

1. Prasad R, Kennedy LA, Ruckenstein E (1984) Catal Rev Sci Eng 26:1
2. Dwyer FG (1972) Catal Rev Sci Eng 6:261
3. Zwinkels MFM, Järås SG, Menon PG, Griffin TA (1993) Catal Rev Sci Eng 35:319
4. Kummer JT (1980) Prog Energy Combust Sci 6:177
5. Cao J-L, Wang Y, Zhang T-Y, Wu S-H, Yuan Z-Y (2008) Appl Catal B 78:120
6. Cao J-L, Wang Y, Yu X-L, Wang S-R, Wu S-H, Yuan Z-Y (2008) Appl Catal B 79:26
7. Luo M-F, Ma J-M, Lu J-Q, Song Y-P, Wang Y-J (2007) J Catal 246:52
8. Ma L, Luo MF, Chen SY (2003) Appl Catal A 242:151
9. Jung CR, Han J, Nam SW, Lim T-H, Hong S-A, Lee H-I (2004) Catal Today 93–95:183
10. Matias J, Fernando M, Betina S, Graciela B, Miguel L (2006) Chem Mater 18:1945
11. Wang S-P, Zheng X-C, Wang X-Y, Wang S-R, Zhang S-M, Yu L-H, Huang W-P, Wu S-H (2005) Catal Lett 105:163
12. Yu Yao YF, Kummer JT (1977) J Catal 46:388
13. Boon AQM, Huisman HM, Geus JW (1992) J Mol Catal 75:293
14. Ozkan US, Kueller RF, Moctezuma E (1990) Ind Eng Chem Res 29:1136
15. Rajesh H, Ozkan US (1993) Ind Eng Chem Res 32:1622
16. Avgouropoulos G, Papavasiliou J, Tabakova T, Idakiev V, Ioannides T (2006) Chem Eng J 124:41
17. Huang J, Wang S, Zhao Y, Wang X, Wang S, Wu S, Zhang S, Huang W (2006) Catal Commun 7:1029
18. Wang JA, Chen LF, Valenzuela MA, Montoya A, Salmoned J, Angel PD (2004) Appl Surf Sci 230:34
19. Si R, Zhang Y-W, Xiao C-X, Li S-J, Lin B-X, Kou Y, Yan C-H (2004) Phys Chem Chem Phys 5:1056
20. Daturi M, Finocchio E, Biinet C, Lavalley JC, Fally F, Perrichon V, Vidal H, Hickey N, Kaspar J (2000) J Phys Chem B 104:9186
21. Masui T, Ozaki T, Machida K, Adachi G (2000) J Alloys Compds 303–304:49
22. Thammachart M, Meeyoo V, Risksomboon T, Osuwan S (2001) Catal Today 68:53
23. Bozo C, Guilhaume N, Garbowski E, Primet M (2000) Catal Today 59:33
24. Trovarelli A, De Leitenburg C, Dolcetti G (1997) ChemTech 27:32
25. Chen HL, Zhu HY, Wu Y, Gao F, Dong L, Zhu JJ (2006) J Mol Catal A 255:254
26. Chen Y-Z, Liaw B-J, Chen H-C (2006) Int J Hydrogen Energy 31:427
27. Ratnasamy P, Srinivas D, Satyanarayana CVV, Manikandan P, Senthil Kumaran RS, Sachin M, Shetti VN (2004) J Catal 221:455
28. Huber F, Yu ZX, Walmsley JC, Chen D, Venvik HJ, Holmen A (2007) Appl Catal B 71:7
29. Wang S-P, Wang X-Y, Huang J, Zhang S-M, Wang S-R, Wu S-H (2007) Catal Comm 8:231
30. Dong X-F, Zou H-B, Lin W-M (2006) Int J Hydrogen Energy 31:2337
31. Ren T-Z, Yuan Z-Y, Su B-L (2003) Chem Phys Lett 374:170
32. Yuan Z-Y, Su B-L (2003) Chem Phys Lett 381:710
33. Lin R, Luo M-F, Zhong Y-J, Yuan Z-L, Liu G-Y, Liu W-P (2003) Appl Catal A 255:331
34. Zhou R-X, Yu T-M, Jiang X-Y, Chen F, Zheng X-M (1999) Appl Surf Sci 148:263
35. Avgouropoulos G, Ioannides T (2003) Appl Catal A 244:155